Journal of Theoretical and Applied Physics (2020) 14:65–74
https://doi.org/10.1007/s40094-019-00360-6

RESEARCH

Investigation of carbon monoxide gas adsorption on the Al_2O_3/$Pd(NO_3)_2$/zeolite composite film

Nastaran Mozaffari[1] · Alireza Haji Seyed Mirzahosseini[1] · Amir Hossein Sari[2] · Leila Fekri Aval[2]

Received: 23 July 2019 / Accepted: 25 November 2019 / Published online: 17 December 2019

Abstract

In this study, Al_2O_3/$Pd(NO_3)_2$/zeolite composite films have been fabricated by roll coating method and characterized by X-ray diffraction, energy-dispersive X-ray spectroscopy and field emission scanning electron microscopy. The gas adsorption was tested in an experimental setup by a continuous gas analyzer KIMO KIGAZ 210 at constant temperature and pressure (32 °C and 1.5 bar) and as a function of reaction time (s). The inlet CO gas concentration was 150 mg L^{-1}, and the saturation level of CO gas concentration was 5 mg L^{-1}. The maximum adsorption capacity (q_{max}) and maximum adsorption efficiency (%) were calculated as 111.16 mg g^{-1} and 97%, respectively. Pseudo-first-order, pseudo-second-order, and intra-particle diffusion models were investigated to kinetic study of CO adsorption on Al_2O_3/$Pd(NO_3)_2$/zeolite adsorbents. Results indicated that CO adsorption follows the pseudo-second-order model well according to regression coefficient value ($R^2 = 0.98$), and the value of pseudo-second-order rate constant of adsorption was obtained as 2×10^{-5} g mg^{-1} s^{-1}. According to the intra-particle diffusion model, adsorption is affected by only one process. So, adsorption of CO by Al_2O_3/$Pd(NO_3)_2$/zeolite adsorbent indicated an effective adsorption by obtained results.

Keywords Carbon monoxide · Adsorption · Zeolite · Palladium II nitrate · Alumina · Kinetic study

Introduction

Carbon monoxide (CO) is an achromatic, odorless and tasteless gas that can be poisonous for humans due to serious threats for the environment including acid rain, ozone depletion and secondary pollutants production [1, 2]. Any burning materials and fuels containing carbon are considered to be the main sources of CO. Wide range of flammable carbon monoxide [3] along with the release of CO mixture in chemical accidents [4] motivated researchers to find effective ways for capturing CO from defective burned atmosphere which is a great improvement in health issues [5]. Therefore, in recent decades, the development of cost-effective technologies for capturing CO has attracted tremendous attentions [6–8].

Various types of porous materials have been applied for CO capture, and it is still full of challenges. Surface properties of porous adsorbents such as well thickness, surface area, and pore-size distribution make their applications increased significantly [9–15] including nanoporous materials such as metal–organic frameworks (MOFs) [16, 17], mesoporous alumina (MA) [18, 19], and mesoporous silica (MS) [20, 21] which are known as an alternative to other commercial adsorbents such as zeolite and activated carbon [22, 23].

Because of the uniform structure of the porous nanomaterials MS, MOFs, and MA and their high surface areas, the adsorption capacity of these adsorbents is significant [24]. Accordingly, high adsorption capacity of alumina-based substances is due to the uniform pore size, interlinked channels, and the united porous structures [25, 26]. The usage of alumina-based materials as a catalyst in purification processes (e.g., hydrotreatment, hydrocracking, and modification), along with their role as adsorbents, in particular, for toxic gases removal, is widely known [27]. Among seven types of alumina phases known as "transition alumina" [28], due to the impurity and defects of their crystal lattice, the stable phase belongs to α-alumina while γ-alumina has

✉ Alireza Haji Seyed Mirzahosseini
a.mirzahosseini@srbiau.ac.ir

[1] Department of Environmental Engineering, Faculty of Natural Resources and Environment, Science and Research Branch, Islamic Azad University, Tehran, Iran

[2] Plasma Physics Research Center, Faculty of Sciences, Science and Research Branch, Islamic Azad University, Tehran, Iran

less stability [29, 30]. γ-Phase nano-Al_2O_3 with large surface area, pore-volume, and high catalytic activity, as one of the most important and newest ceramic materials, is the best candidate for capturing gas molecules, as the same as mesoporous alumina (MA) [31, 32]. Therefore, herein, the γ-phase nano-Al_2O_3 has been used as the base substance. Remarkable progress has been carried out in the past few years for γ-Al_2O_3 synthesis [33].

In addition, the development of palladium (Pd) and palladium (II) nitrate nanoparticles is an important issue due to their applications as catalysis, water denitrification and CO gas adsorption because of their remarkable properties [34] along with their superior performances [35, 36] due to their tiny uniform pores [37]. The smaller particle size of Pd clusters on the surface of Al_2O_3 favors a higher CO adsorption and enhances the adsorption capacity of the adsorbent.

Moreover, zeolite (Ze) nanoparticles are considered as crystalline aluminosilicates (or silicates) with two-dimensional regular arrangements of pores. Zeolite nanoparticles have unique properties such as high surface areas, exchangeable cations, molecular sieving [38].

Hence, as the major aim of the present study, $Pd(NO_3)_2$, zeolite and Al_2O_3 were loaded on glass substrates by roll coating technique to improve the ability of adsorbents for CO adsorption and increase the range of reactions between CO gas molecules and adsorbents surface. In addition, the adsorption capacity and efficiency of $Al_2O_3/Pd(NO_3)_2$/zeolite composite films were calculated which are equal to 111.16 (mg g^{-1}) and 97%, respectively, and also adsorption kinetic mechanism was studied by pseudo-first-order, pseudo-second-order, and intra-particle diffusion models. The morphology has been probed by field emission scanning electron microscopy (FESEM), and structural properties were also explored by X-ray diffraction (XRD).

Experimental details

Adsorption of CO

Here, CO (99,999%) was used as a target gas. The schematic of designed and made experimental setup for measuring CO adsorption is given in Fig. 1. As can be seen from Fig. 1, the set up consists of a capsule as a source of CO gas, the compartment (20 cm length and 7 cm internal diameter), in which an adsorbent is putted, and a gas analyzer apparatus (KIMO KIGAZ 210) for evaluating CO gas concentration. In this study, temperature and pressure were held constant at 32 °C (at room temperature) and 1.5 bar, respectively. The inlet CO gas concentration was 150 mg L^{-1}, and the saturation level of CO gas concentration was 5 mg L^{-1}.

Materials

Zeolite nanoparticles ($Al_2O_34SiO_2H_2O$, purity: > 99%) and alumina nanoparticles (Al_2O_3, gamma, purity: > 99.9%) were purchased from Nanoshel chemicals. Palladium nitrate ($Pd(NO_3)_2$) and 1-methyl-2-pyrrolidone were bought from Sigma-Aldrich and Merck chemicals, respectively. All received chemicals were used without extra purification.

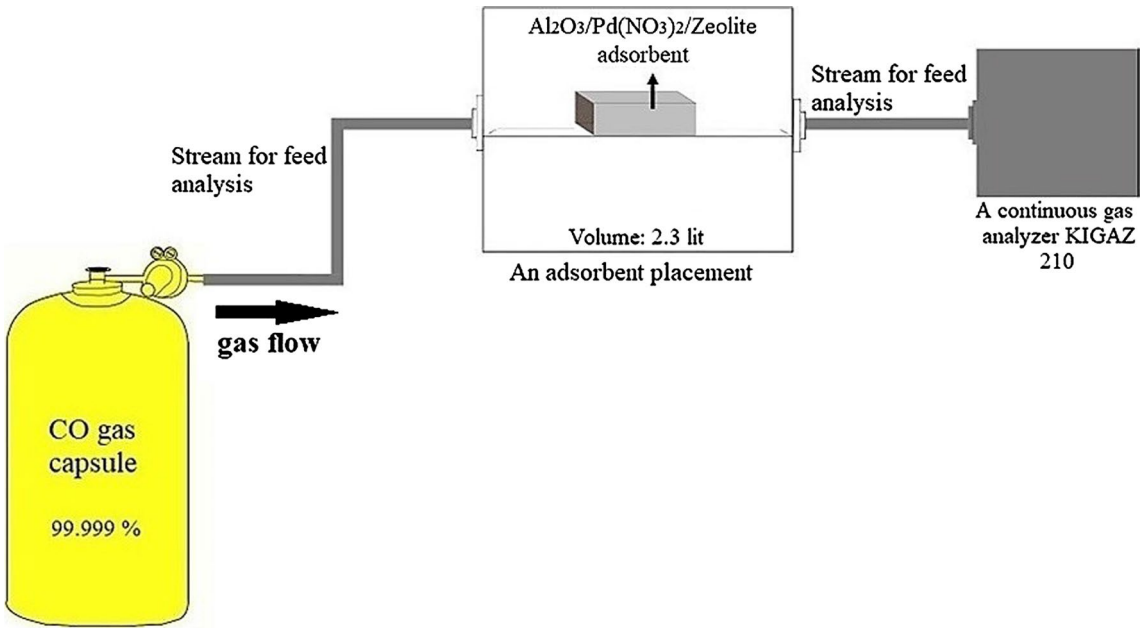

Fig. 1 Schematic of the experimental setup used for CO gas adsorption testing on $Al_2O_3/Pd(NO_3)_2$/zeolite composite film consists of CO gas capsule (purity = 99.999%), an adsorbent placement, a gas analyzer device (KIMO KIGAZ 210)

Preparation of adsorbent

$Al_2O_3/Pd(NO_3)_2$/zeolite composite films have been deposited on glass substrates by roll coating method. Four glass substrates (2 cm × 8 cm) were washed three times by disinfectant materials such as acetone, ethanol, and deionized water in an ultrasonic device and dried at room temperature. The process of preparation of samples was including 1 gr Al_2O_3: 1 gr zeolite: 1 gr $Pd(NO_3)_2$ mixed in a small container, and then, 10 CC of 1-methyl-2-pyrrolidone was slowly added dropwise into it. Final suspensions were stirred for about 1 h and then used for coating on glasses. The prepared coated substrates were desiccated at room temperature for 1 day. Finally, four $Al_2O_3/Pd(NO_3)_2$/zeolite-coated substrates were attached together to make a hollow cubic container as shown in Fig. 2, to study CO adsorption on $Al_2O_3/Pd(NO_3)_2$/zeolite composite films. In this case, it behaves as a tunnel in which gas molecules are channeled and trapped readily. Thus, the rate of interaction between gas molecules and adsorbents is enhanced which will affect the adsorption capacity and efficiency.

Characterization

The structural and morphological properties of $Al_2O_3/Pd(NO_3)_2$/zeolite composite film were characterized. The crystalline structure of the composite film was analyzed by X-ray diffraction (XRD, STOE STADI MP). The visualization of topography and morphology of prepared samples were analyzed by field emission scanning electron microscope (FESEM, MIRA3 TESCAN), while chemical and elemental contents of the sample were measured by energy-dispersive X-ray spectroscopy (EDX) analysis system attached with scanning electron microscope. The thickness of the prepared sample was determined by profilometer analysis (RAGA). The gas analyzer device (KIMO KIGAZ 210) was applied for CO gas adsorption test.

Results and discussion

XRD

Figure 3 shows the XRD patterns of $Al_2O_3/Pd(NO_3)_2$/zeolite adsorbent. XRD patterns were recorded using an X-ray diffractometer with Cu $K\alpha$ source ($\lambda = 1.5405$ Å) and a scan step size of 0.01°. The scanning range (2θ) was recorded between 10° and 90°. The XRD peaks of the composite film were considered at 10.98°, 13.05°, 17.23°, 22.31°, 25°, 29°, 37°, 44.50°, 46.22°, 51.73°, 57.45°, which were assigned to the crystalline preferred orientation of 220, 110, 121, 200, 040, 125, 110, 323, 202, 420, 116, respectively (Table 1). As can be seen in the XRD patterns, the adsorbent shows three major peaks (at $2\theta = 22.31°$, 29°, 44.50°) due to the presence of zeolite and palladium II nitrate.

D_{XRD} was used to find the size of nanoparticles from Debye–Scherrer's equation and XRD [39–41] (1):

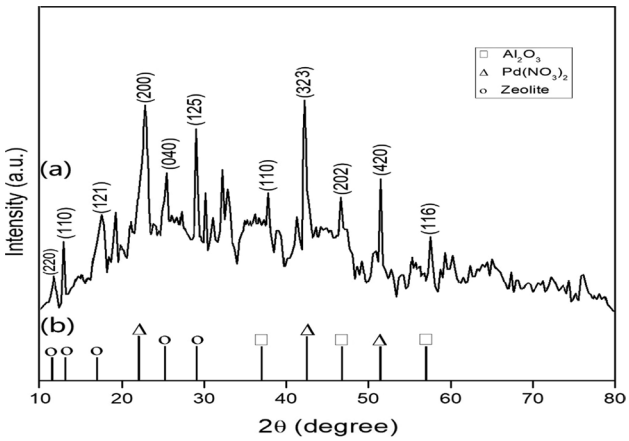

Fig. 3 XRD patterns of **a** the $Al_2O_3/Pd(NO_3)_2$/zeolite composite film, **b** reference γ-Al_2O_3 (JCPDS 00-011-0661), $Pd(NO_3)_2$ (JCPDS 00-001-0398) and zeolite (JCPDS 00-042-0018 and 01-087-2276) nanoparticles

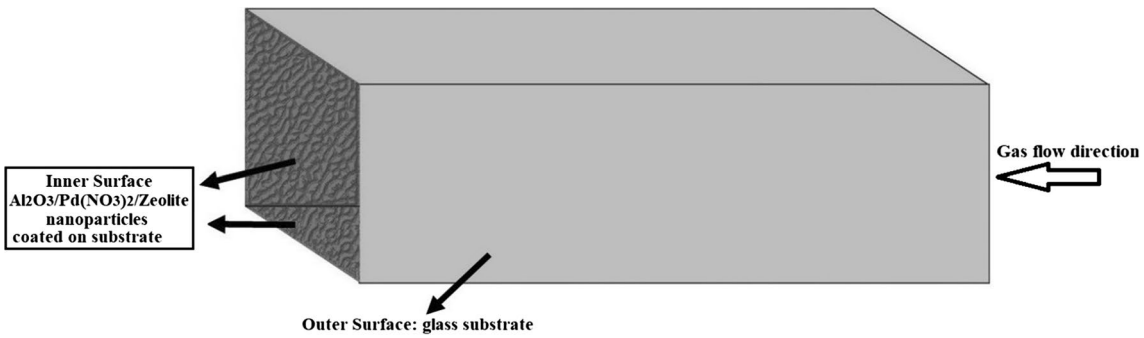

Fig. 2 Schematic of fabricated $Al_2O_3/Pd(NO_3)_2$/zeolite adsorbent in the form of cubic

Table 1 XRD peaks and crystalline areas of the $Al_2O_3/Pd(NO_3)_2$/zeolite composite film

Samples	Zeolite	Zeolite	Zeolite	$Pd(NO_3)_2$	Zeolite	Zeolite	Al_2O_3	$Pd(NO_3)_2$	Al_2O_3	$Pd(NO_3)_2$	Al_2O_3
hkl	220	110	121	200	040	125	110	323	202	420	116
2θ (Degree)	10.98	13.05	17.23	22.31	25	29	37	44.50	46.22	51.73	57.45

Table 2 Particle diameters of Al_2O_3, $Pd(NO_3)_2$, zeolite

Samples	Al_2O_3		$Pd(NO_3)_2$	Zeolite
hkl	(202)	(116)	(323)	(123)
FWHM	0.9446	0.6298	0.3936	0.3149
D_{XRD}(nm)	9	14	22	26

$$D_{\mathrm{XRD}} = \frac{K\lambda}{\beta \mathrm{Cos}(\theta)} \tag{1}$$

where K is known as the shape factor or Scherrer's constant that varies in the range $0.89 < K < 1$, and usually is 0.9 (assuming that the particles have spherical shape), λ is the X-ray wavelength (1.54178 Å), β is full width at half maximum (FWHM) of the diffraction peak and θ is the diffraction angle. The particle diameters of the samples are summarized in Table 2.

FESEM

In order to determine surface morphology, particle size and distribution of the prepared adsorbent, field emission scanning electron microscope (FESEM) analysis was employed. FESEM images of $Al_2O_3/Pd(NO_3)_2$/zeolite sample at 200 nm scale of magnification before and after CO gas adsorption are presented in Fig. 4.

The development of united porous structures with regular interlinked channels is observable in the adsorbent after adsorption. As it is obvious, the FESEM image after adsorption represents more homogeneous dispersion and well particle size repartition in respect to the virgin film. These properties are responsible for the high surface area and therefore very high adsorption for CO. The average size of particles is equal to 37.41 nm. The result from the profilometer analysis determined that the thickness of the $Al_2O_3/Pd(NO_3)_2$/zeolite composite film is 6966.7 nm.

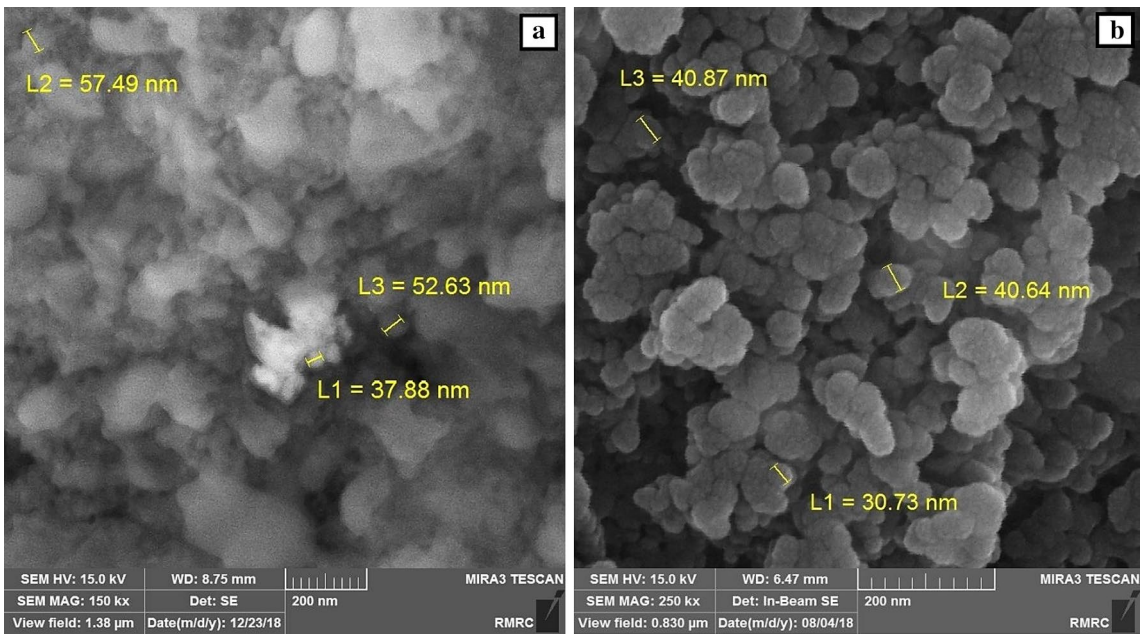

Fig. 4 FESEM images of the made adsorbent with $Al_2O_3/Pd(NO_3)_2$/zeolite nanoparticles **a** before and **b** after CO gas adsorption at 200 nm scales of magnification

EDX

Energy-dispersive X-ray spectroscopy (EDX) was carried out to determine the percentage of elemental content. EDX pattern in Fig. 5 confirms the presence of the ingredients which were utilized as adsorbents. The spectrum of the droplets shows a notable increase at the spectral position of Al EDX peak. The increase of aluminum peak is due to the use of alumina nanoparticles and zeolite (aluminosilicates) nanoparticles in this study. Table 3 reveals the weight and atomic percentages of ingredients extracted from EDX patterns of the adsorbent including Al, O, Pd as well as N and Si at 32.57, 55.16, 1.57, 4.10, 7.59 wt% for each element. In addition, Ca peak corresponded to glass substrates [42].

Adsorption of CO

The variation of concentration of adsorbed CO versus time for $Al_2O_3/Pd(NO_3)_2$/zeolite adsorbent at constant temperature and pressure is shown in Fig. 6. As can be seen, the concentration of adsorbed CO gas (mg L^{-1}) is increased with increasing time (s). However, the decrease of slope indicates that the adsorption speed became lower since it reaches saturation region.

The adsorption efficiency ($R\%$) which specifies the performance of adsorbent for CO adsorption, adsorption capacity at time t (q_t, mg g^{-1}), and adsorption capacity (q_e, mg g^{-1}) which evaluates the concentration of adsorbed CO gas through the adsorbent at equilibrium were calculated by using Eqs. (2), (3), and (4), respectively [43]:

$$R = \frac{(C_0 - C_e)}{C_0} \times 100 \tag{2}$$

$$q_t = \frac{(C_0 - C_t) \times V}{M} \tag{3}$$

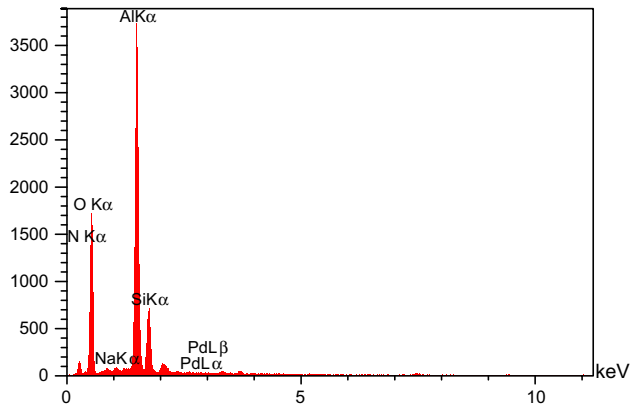

Fig. 5 EDX result of the $Al_2O_3/Pd(NO_3)_2$/zeolite composite film

Table 3 Atomic and weight percentage values of the $Al_2O_3/Pd(NO_3)_2$/zeolite composite film by statistical analysis of EDX spectrum

Elements	wt%	at%
N Ka	4.10	5.59
O Ka	55.16	65.83
Al Ka	32.57	23.05
Si Ka	7.59	5.16
Ca Ka	1.52	0.88
Pd La	1.57	0.34

$$q_e = \frac{(C_0 - C_e) \times V}{M} \tag{4}$$

where C_0 (mg L^{-1}) is the inlet concentration, C_t (mg L^{-1}) is concentration of adsorbed CO gas at time t, C_e (mg L^{-1}) is concentration of adsorbed CO gas at equilibrium, $V(L)$ is the volume of the chamber, and $M(g)$ is the weight of the adsorbent.

The variation of adsorption efficiency ($R\%$) versus time for CO gas adsorption on $Al_2O_3/Pd(NO_3)_2$/zeolite adsorbent is shown in Fig. 7. As can be seen, the adsorption efficiency is increased with increasing time (s). The maximum percentage of CO adsorption is equal to 97% which occurred at 216 (s), and then, a saturation region was developed indicating that vacant sites in $Al_2O_3/Pd(NO_3)$/zeolite are saturating with CO molecules while time is passing [44].

Figure 8 shows the variation of adsorption efficiency versus concentration of adsorbed CO gas which is a single, smooth, and linear curve. It demonstrates that efficiency is increased by increasing the concentration of adsorbed CO gas, and it is continuous until it leads to a saturation region.

Figure 9 shows adsorption capacity (q_t, mg g^{-1}) versus time (s) diagram. The results revealed obvious enhancing in

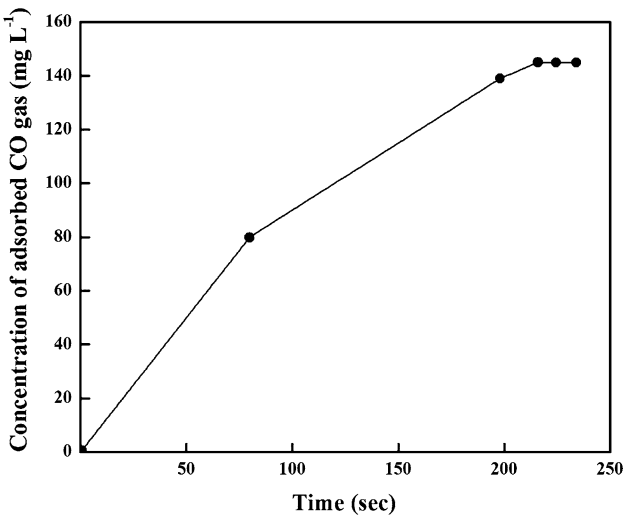

Fig. 6 The diagram of the concentration of adsorbed CO gas (mg L^{-1}) as a function of time (s)

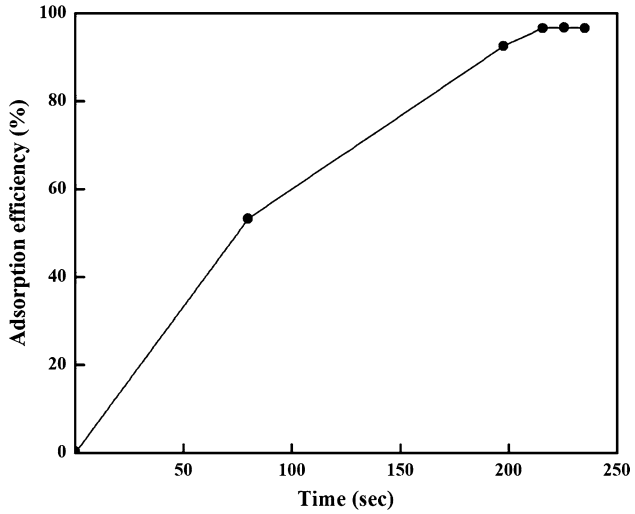

Fig. 7 The adsorption efficiency (%) of CO gas as a function of time (s) curve

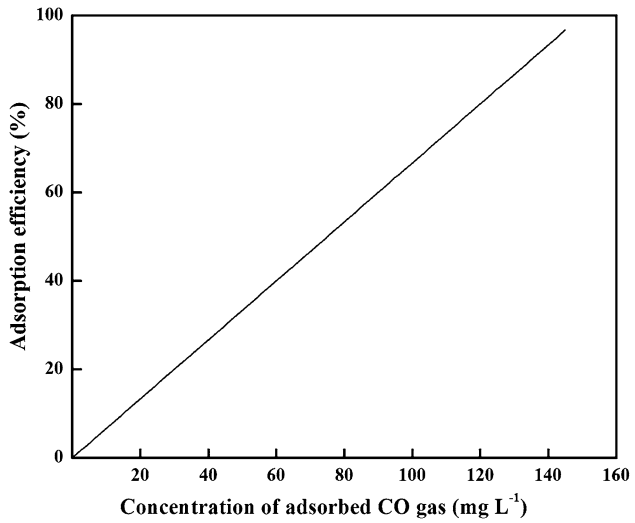

Fig. 8 The effect of outlet CO gas concentration (mg L^{-1}) on adsorption efficiency (%)

the adsorption capacity of $Al_2O_3/Pd(NO_3)_2$/zeolite adsorbent for CO adsorption with the increase of time (s). The maximum adsorption capacity is 111.16 mg g^{-1}. Also, at this point, the saturation point was started and defined as "adsorption capacity at equilibrium time." This means that adsorption sites were saturated with CO molecules, and there are no other sites to attach to CO molecules with increasing time [45].

Table 4 gives adsorption capacity, adsorption efficiency, inlet gas concentration, and concentration at the saturation level of CO gas adsorption results on $Al_2O_3/Pd(NO_3)_2$/zeolite film. According to Table 5, by comparing with other published articles, the results indicate that adsorption

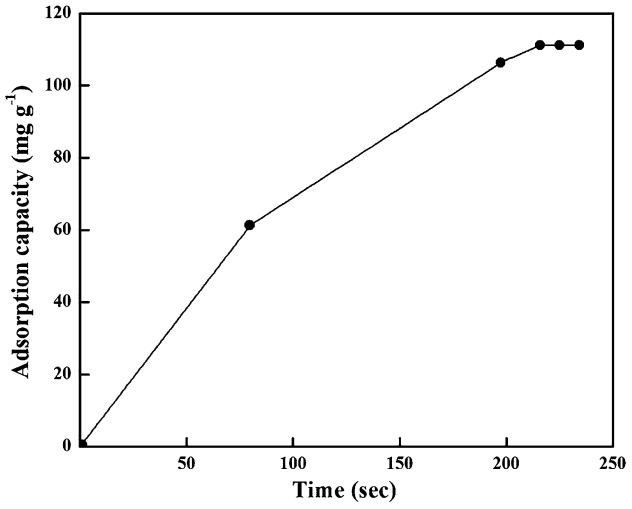

Fig. 9 The relation between time (s) and the uptake capacity (mg g^{-1})

Table 4 Parameters of adsorption capacity and adsorption efficiency for CO gas on $Al_2O_3/Pd(NO_3)_2$/zeolite composite film at room temperature (32 °C)

Initial CO gas concentration (mg L^{-1})	Saturation point of CO gas concentration (mg L^{-1})	Maximum of adsorption capacity q_{max} (mg g^{-1})	Maximum of the adsorption efficiency (%)
150	5	111.16	97%

Table 5 Comparison of adsorption capacity parameters for CO gas on $Al_2O_3/Pd(NO_3)_2$/zeolite composite film and various adsorbents at room temperature (32 °C)

Samples	Q_m (mg g^{-1}) at room temperature	Reference
$Al_2O_3/Pd(NO_3)_2$/zeolite	111.16	Current work
Pd/MA	228.5	[20]
MA	170.4	[20]
Pd/AC	77.6	[20]
Pd/Si	34.6	[20]
Ze	28.3	[20]
Si	26.8	[20]
AC	25.2	[20]

capacity of $Al_2O_3/Pd(NO_3)_2$/zeolite composite film is higher than Ze, Si, AC, Pd/Si and Pd/AC adsorbents, and lower than MA and Pd/MA adsorbents [20].

Kinetic study

The pseudo-first-order, pseudo-second-order and intra-particle diffusion models are applied to analyze the kinetic

study of CO gas adsorption on $Al_2O_3/Pd(NO_3)_2$/zeolite composite films.

Pseudo-first- order kinetic

Pseudo-first-order model is applicable to study adsorption process during the initial stage [46–48]. The pseudo-first-order model (Lagergen, 1898) [49] is defined as Eq. (5):

$$\log\left(q_e - q_t\right) = \log q_e - \frac{K_{\text{ad}}}{2.303}t \tag{5}$$

By determining the intercept ($\log q_e$) and slope ($\frac{K_{\text{ad}}}{2.303}$) of a linear plot of $\log\left(q_e - q_t\right)$ vs. t, calculated equilibrium adsorption density (q_e) and pseudo-first-order constant (K_{ad}) can be calculated [46]. Figure 10 shows a linear plot of $\log\left(q_e - q_t\right)$ versus time. According to Table 6, the experimental value of $q_{e,\text{exp}}$ is not agreement with the theoretical value of $q_{e,\text{cal}}$. The regression coefficient (R^2) is 0.86. Therefore, the low values of R^2 and negative slope of $\log\left(q_e - q_t\right)$ vs. t indicate the inadequacy of the pseudo-first-order model to describe interaction among $Al_2O_3/Pd(NO_3)_2$/zeolite molecules [50].

Pseudo-second -order kinetic

In order to investigate the influence of chemical potential of adsorbent which is sensitive to temperature, time and gas concentration on adsorption process, the pseudo-second-order model is applied [45, 48, 51]. The equation related to pseudo-second order is given as [46, 52]:

$$\frac{t}{q_t} = \frac{1}{k_2 q_e^2} + \frac{t}{q_e} \tag{6}$$

The linear $\frac{t}{q_t}$ versus t plot gives intercept $\frac{1}{k_2 q_e^2}$ and slope $\frac{1}{q_e}$ to determine pseudo-second-order constant (K_2, g mg^{-1} s^{-1}) and theoretical $q_{e,\text{cal}}$ calculated value [46]. Figure 11 indicates a linear plot of $\frac{t}{q_t}$ versus t for $Al_2O_3/Pd(NO_3)_2$/zeolite composite films which remained stable until 80 s and then increased with passing time.

Kinetic parameters of $Al_2O_3/Pd(NO_3)_2$/zeolite adsorbent are given in Table 6. The experimental and theoretical values of q_e are not in agreement with each other. Also, the smaller value of K_2 than $K_2 q_e^2$ (initial rate constant) indicates the fast CO adsorption process during the initial period of time, and then, it was getting slower with time [47, 53]. The value of regression coefficient (R^2) for this

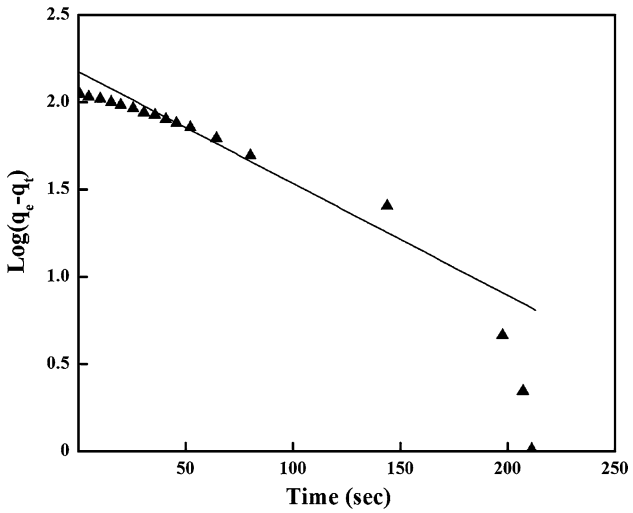

Fig. 10 Pseudo-first-order kinetic model for CO adsorption by $Al_2O_3/Pd(NO_3)_2$/zeolite composite films

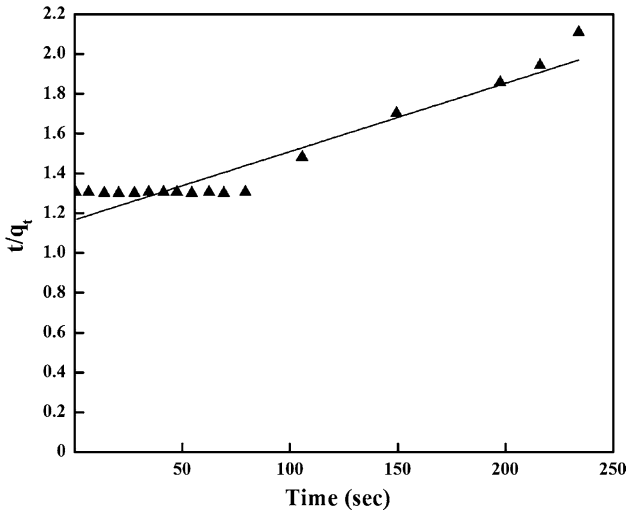

Fig. 11 Pseudo-second-order kinetic model for CO adsorption by $Al_2O_3/Pd(NO_3)_2$/zeolite composite films

Table 6 Comparison of pseudo-first-order, pseudo-second-order and intra-particle diffusion models parameters

$q_{e,\text{exp}}$ (mg g^{-1})	Pseudo-first-order kinetic model			Pseudo-second-order kinetic model			Intra-particle diffusion kinetic model
111.09	K_{ad}	$q_{e,\text{cal}}$	R^2	K_2	$q_{e,\text{cal}}$	R^2	K_{diff}
	0.0147	147.91	0.86	2×10^{-5}	222.71	0.98	8.95

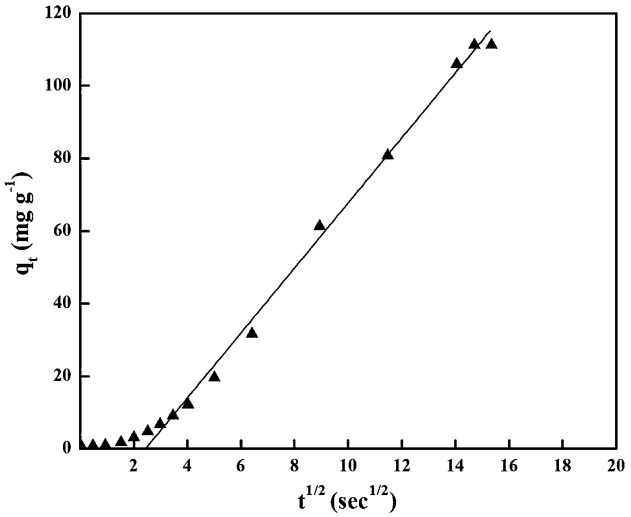

Fig. 12 Intra-particle diffusion kinetic model for CO adsorption by $Al_2O_3/Pd(NO_3)_2$/zeolite composite films

model is close to unity that it is applicable to explain CO adsorption by $Al_2O_3/Pd(NO_3)_2$/zeolite adsorbent [46, 54].

Intra-particle diffusion kinetic model

The intra-particle diffusion kinetic model is a common model to characterize diffusion mechanism of CO molecules and $Al_2O_3/Pd(NO_3)_2$/zeolite composite films. The intra-particle model is defied by Eq. (7) [46, 55]:

$$q_t = K_{\text{diff}} t^{1/2} + C \tag{7}$$

where K_{diff} (mg g^{-1} sec$^{1/2}$) is intra-particle diffusion constant which can be obtained by the slope of the q_t vs. $t^{1/2}$ plot [46] (Fig. 12).

According to the published articles [44, 56–58], the linear plot of q_t vs. $t^{1/2}$ for $Al_2O_3/Pd(NO_3)_2$/zeolite adsorbents through the whole time process shows that adsorption is affected by only one proceeding. Also, intra-particle diffusion is a rate-controlling step because the plot passes through the origin [56, 57]. Table 6 gives value of intra-particle diffusion constant.

Conclusion

The present study aimed to improve CO adsorption through adsorbent and increase the range of interactions between CO gas molecules and adsorbent. Therefore, the roll coating technique was applied for the preparation of $Al_2O_3/Pd(NO_3)_2$/zeolite composite films through loading $Pd(NO_3)_2$, zeolite and Al_2O_3 nanoparticles on glass substrates. While the inlet CO gas concentration was 150 mg L^{-1}, adsorbed CO gas concentration was calculated as a function of reaction time. The concentration of adsorbed CO gas was increased by passing time until 216th seconds and then it reached a saturation level of 5 mg L^{-1} due to the increase of contact surface area of adsorbent particles with CO gas molecules. Moreover, adsorption efficiency ($R\%$) which showed the performance of adsorbent for CO adsorption was increased by increasing time and increasing concentration of adsorbed CO gas until it reached the saturation level with the maximum value of 97%. Uptake capacity (q_t) was also defined to evaluate the concentration of adsorbed CO through the adsorbent and increased with the increase of time and remained nearly constant with slight changes by increasing time with the maximum value of 111.16 mg g^{-1}. Kinetic study was investigated by pseudo-first-order, pseudo-second-order, and intra-particle diffusion models. CO adsorption process was the best fit by pseudo-second-order model with the high value of R^2 (0.98). CO adsorption occurred through one step according to intra-particle diffusion model. Also, intra-particle diffusion is rate-controlling step because the plot passes through the origin. Elemental content of Al, O, Pd, Si, and N as well as Ca which was referred to glass substrates was observed in EDX analysis while the crystalline structure of $Al_2O_3/Pd(NO_3)_2$/zeolite composite films with their particles diameters and FWHM was characterized through XRD patterns. The interconnected channels in the structures of $Al_2O_3/Pd(NO_3)_2$/zeolite surfaces in FESEM images with united porous structures are responsible for the efficient capture of CO gas molecules. Moreover, homogeneous dispersion and well particle size repartition of $Al_2O_3/Pd(NO_3)_2$/zeolite adsorbent with the average size of 37/41 nm were obtained.

Acknowledgements This research work was supported by the Science and Research Branch, Islamic Azad University, Tehran, Iran.

References

1. Sandilands, E.A., Bateman, D.N.: Carbon monoxide. Medicine (2016). https://doi.org/10.1016/j.mpmed.2015.12.024

2. Berea, E., Montoro, C., Navarro, J.A.R.: Toxic gas removal—metal–organic frameworks for the capture and degradation of toxic gases and vapor. Chem. Soc. Rev. (2014). https://doi.org/10.1039/C3CS60475F
3. Goldstein, M.: Carbon monoxide poisoning. J. Emerg. Nurs. (2008). https://doi.org/10.1016/j.jen.2007.11.014
4. Raub, J.: World Health Organization & International Programme on Chemical Safety, Carbon Monoxide, 2nd ed. World Health Organization (1999). https://apps.who.int/iris/handle/10665/42180
5. Glover, T.G., Peterson, G.W., Schindler, B.J., Britt, D., Yagi, O.: MOF-74 building unit has a direct impact on toxic gas adsorption. Chem. Eng. Sci. (2011). https://doi.org/10.1016/j.ces.2010.10.002
6. Yin, X., Dastan, D., Wu, F., Li, J.: Facile synthesis of SnO_2/$LaFeO_3$ – XNX composite: photocatalytic activity and gas sensing performance. Nanomaterials (2019). https://doi.org/10.3390/nano9081163
7. Mozaffari, N., Elahi, S.H., Parhizgar, S.S., Mozaffari, N., Elahi, S.M.: The effect of annealing and layer numbers on the optical and electrical properties of cobalt-doped TiO_2 thin films. Mater. Res. Express (2019). https://doi.org/10.1088/2053-1591/ab4662
8. Yin, X., Zhou, W.D., Li, J., Wang, Q., Wu, F.Y., Dastan, D., Wang, D., Garmestani, H., Wang, X.M., Talu, S.: A highly sensitivity and selectivity Pt-SnO_2 nanoparticles for sensing applications at extremely low level hydrogen gas detection. J Alloys Compd. (2019). https://doi.org/10.1016/j.jallcom.2019.07.081
9. Yin, X.T., Zhou, W.D., Li, J., Lv, P., Wang, Q., Wang, D., Wu, F.Y., Dastan, D., Garmestani, H., Shi, Z., Ţălu, S.: Tin dioxide nanoparticles with high sensitivity and selectivity for gas sensors at sub ppm level of hydrogen gas detection. J. Mater. Sci.: Mater. Electron. (2019). https://doi.org/10.1007/s10854-019-01840-w
10. Hung, C.-T., Bai, H.: Adsorption behaviors of organic vapors using mesoporous silica particles made by evaporation induced self-assembly method. Chem. Eng. Sci. (2008). https://doi.org/10.1016/j.ces.2008.01.002
11. Serrano, D.P., Calleja, G., Botas, J.A., Gutierrez, F.J.: Characterization of adsorptive and hydrophobic properties of silicalite-1, ZSM-5, TS-1 and beta zeolites by TPD techniques. Sep. Purif. Techol. (2007). https://doi.org/10.1016/j.seppur.2006.08.013
12. Zare, M., Solaymani, S., Shafiekhani, A., Kulesza, S., Ţălu, S., Bramowicz, M.: Evolution of rough-surface geometry and crystalline structures of aligned TiO_2 nanotubes for photoelectrochemical water splitting. Sci. Rep. (2018). https://doi.org/10.1038/s41598-018-29247-3
13. Talu, S., Bramowicz, M., Kulesza, S., Shafiekhani, A., Ghaderi, A., Mashayekhi, F., Solaymani, S.: Microstructure and tribological properties of Fe NPs @ a-C: H films by micromorphology analysis and fractal geometry. Ind. Eng. Chem. Res. (2015). https://doi.org/10.1021/acs.iecr.5b02449
14. Ţălu, S., Bramowicz, M., Kulesza, S., Ghaderi, A., Dalouji, V., Solaymani, S., Khalaj, Z.: Microstructure and micromorphology of Cu/Co nanoparticles: surface texture analysis. Electron. Mater. Lett. (2016). https://doi.org/10.1007/s13391-016-6036-y
15. Talu, S., Bramowicz, M., Kulesza, S., Dalouji, V., Solaymani, S., Valedbagi, S.: Fractal features of carbon–nickel composite thin films. Microsc. Res. Tech. (2016). https://doi.org/10.1002/jemt.22779
16. Bobbitt, N.S., Mendonca, M.L., Howarth, A.J., Islamoglu, T., Hupp, J.T., Farha, O.K., Snurr, R.Q.: Metal–organic frameworks for the removal of toxic industrial chemicals and chemical warfare agents. Chem. Soc. Rev. (2017). https://doi.org/10.1039/C7CS00108H
17. Britt, D., Tranche Montagne, D., Yaghi, O.M.: Metal–organic frameworks with high capacity and selectivity for harmful gases. Proc. Natl. Acad. Sci. USA (2008). https://doi.org/10.1073/pnas.0804900105
18. Lehman, S.E., Larsen, S.C.: Zeolite and mesoporous silica nanomaterials: greener syntheses, environmental applications and biological toxicity. Environ. Sci.: Nano (2014). https://doi.org/10.1039/C4EN00031E
19. Moitra, N., Trens, P., Raehm, L., Durand, J.O., Cattoen, X., Wong Chi Man, M.: Facile route to functionalized mesoporous silica nanoparticles by click chemistry. J. Mater. Chem. (2011). https://doi.org/10.1039/c1jm12066b
20. Yeom, C., Kim, Y.: Mesoporous alumina with high capacity for carbon monoxide adsorption. Korean J. Chem. Eng. (2017). https://doi.org/10.1007/s11814-017-0309-5
21. Walcarius, A., Mercier, L.: Mesoporous organosilicon adsorbents: Nano engineered materials for removal of organic and inorganic pollutants. J. Mater. Chem. (2010). https://doi.org/10.1039/B924316J
22. Yeom, C., Selvaraj, R., Kim, Y.: Preparation of nonporous alumina using aluminum chloride via precipitation templating method for CO adsorbent. J. Ind. Eng. Chem. (2017). https://doi.org/10.1016/j.jiec.2018.06.023
23. Li, Z., Barnes, J.C., Bosoy, A., Stoddart, J.F., Zink, J.I.: Mesoporous silica nanoparticles in biomedical applications. Chem. Soc. Rev. (2012). https://doi.org/10.1039/C1CS15246G
24. Chen, C., Ann, W.S.: CO_2 capture using mesoporous alumina prepared by a sol–gel process. Chem. Eng. J. (2011). https://doi.org/10.1016/j.cej.2010.11.038
25. Rengaraj, S., Kim, Y., Yeon, J.-W., Kim, W.-H.: Application of Mg-mesoporous alumina prepared by using magnesium stearate as a template for the removal of nickel: kinetics, isotherm, and error analysis. Ind. Eng. Chem. Res. (2007). https://doi.org/10.1021/ie060994n
26. Dejam, L., Solaymani, S., Achour, A., Stach, S., Talu, S., Beryani Nezafat, N., Dalouji, V., Shokri, A.A., Ghaderi, A.: Correlation between surface topography, optical band gaps and crystalline properties of engineered AZO and CAZO thin films. Chem. Phys. Lett. (2019). https://doi.org/10.1016/j.cplett.2019.01.042
27. Thote, J.A., Chatti, R.V., Iyer, K.S., Kumar, V., Valechha, A.N., Labhsetwar, N.K., Biniwale, R.B., Yankee, M.K.N., Rayalu, S.S.: N-doped mesoporous alumina for adsorption of carbon dioxide. J. Environ. Sci. (2012). https://doi.org/10.1016/S1001-0742(11)61022-X
28. Souza Santos, P., Souza Santos, H., Toledo, S.P.: Standard transition alumina. Electron microscopy studies. Mat. Res. **10**, 11 (2000). https://doi.org/10.1590/S1516-14392000000400003
29. Macêdo, M., Bertran, C., Osawa, C.: Kinetics of the $\gamma \rightarrow \alpha$ -alumina phase transformation by quantitative X-ray diffraction. J. Mater. Sci. (2007). https://doi.org/10.1007/s10853-006-1364-1
30. Shek, C.H., Lai, J.K.L., Gu, T.S., Lin, G.M.: Transformation evolution and infrared absorption spectra of amorphous and crystalline nano-Al_2O_3 powders. Nanostruct. Mater. (1997). https://doi.org/10.1016/S0965-9773(97)00201-8
31. Euzen, F.P., Raybaud, P., Krokidis, X., Toulhoat, H., LeLoarer, J.L., Jolivet, J.P., Froidefond, C., Schüth, F., Sing, K.S.W., Weitkamp, J.: Alumina—Handbook of Porous Solids. Wiley, Hoboken (2002)
32. Trueba, M., Trasatti, S.P.: γ-Alumina as a support for catalysts: a review of fundamental aspects. Eur. J. Inorg. Chem. (2005). https://doi.org/10.1002/ejic.200500348
33. Xiao-lan, S., Peng, Q., Hai-pin, Y., Xi, H., Guan-zhou, Q., Synthesis of γ-Al_2O_3 nanoparticles by chemical precipitation method, J. CENT. SOUTH UNIV. TECHNOL. (2005). 1005 - 9784(2005)05 - 0536 – 06
34. Zhang, J., Li, H., Jiang, Z., Xie, Z.: Size and Shape Controlled Synthesis of Pd Nano crystals. Phys. Sci. Rev. (2018). https://doi.org/10.1515/psr-2017-0101
35. Narayanan, R., El-Sayed, M.A.: Catalysis with transition metal nanoparticles in colloidal solution: nanoparticle shape dependence

and stability. J. Phy. Chem. B. (2005). https://doi.org/10.1021/jp051066p
36. Long, R., Rao, Z., Mao, K., Li, Y., Zhang, C., Liu, Q., Wang, C., Li, Z.Y., Wu, X., Xiong, Y.: Efficient coupling of solar energy to catalytic hydrogenation by using well-designed palladium nanostructures. Angew. Chem. (2015). https://doi.org/10.1002/anie.201407785
37. Wu, J., Zeng, L., Cheng, D., Chen, F., Zhan, X., Gong, J.: Synthesis of Pd nanoparticles supported on CeO_2 nanotubes for CO oxidation at low temperatures. Chin. J. Catal. (2016). https://doi.org/10.1016/S1872-2067(15)60913-5
38. Page, M.P., Mikel, J., Guan, K., Zhang, S., Tringe, J., Castro, R.H.R., Stroeve, P.: Gas adsorption properties of ZSM-5 zeolites heated to extreme temperatures. Ceram. Int. (2016). https://doi.org/10.1016/j.ceramint.2016.06.193
39. Alexander, L., Klug, H.P.: Determination of Crystallite Size with the X-Ray Spectrometer. J. Appl. Phys. (1950). https://doi.org/10.1063/1.1699612
40. Jbara, A.S., Othaman, Z., Ati, A.A., Saeed, M.A.: Characterization of γ- Al_2O_3 nanopowders synthesized by Co-precipitation method. Mater. Chem. Phys. (2017). https://doi.org/10.1016/j.matchemphys.2016.12.015
41. Yin, X.T., Zhou, W.D., Li, J., Lv, P., Wang, Q., Wang, D., Wu, F.Y., Dastan, D., Garmestani, H., Shi, Z., Talu, S.: Tin dioxide nanoparticles with high sensitivity and selectivity for gas sensors at sub-ppm level of hydrogen gas detection. J. Mater. Sci.: Mater. Electron. (2019). https://doi.org/10.1007/s10854-019-01840-w
42. Mozaffari, N., Elahi, S.M., Parhizgar, S.S.: Deposition of TiO_2 multilayer thin films doped with cobalt and studying the effect of annealing temperatures and number of layers on the structural and morphological of thin films. Int. J. Thermophys. (2019). https://doi.org/10.1007/s10765-019-2533-1
43. Tabesh, S., Davar, F., Estarki, M.R.L.: Estarki, Preparation of γ-Al_2O_3 nanoparticles using modified sol-gel method and its use for the adsorption of lead and cadmium ions. J. Alloys Compd. (2018). https://doi.org/10.1016/j.jallcom.2017.09.246
44. Samandari, S.S., Gulcan, H.O., Samandari, S.S., Gazi, M.: Efficient Removal of Anionic and Cationic Dyes from an Aqueous Solution Using Pullulan-graft-Polyacrylamide Porous Hydrogel. Water Air Soil Pollut. (2014). https://doi.org/10.1007/s11270-014-2177-5
45. Mungondori, H.H., Mtetwa, S., Tichagwa, L., Katwire, D.M., Nyamukamba, P.: Synthesis and application of a ternary composite of clay, saw-dust and peanut husks in heavy metal adsorption. Water Sci. Technol. (2017). https://doi.org/10.2166/wst.2017.123
46. Tanhaei, B., Ayati, A., Lahtinen, M., Sillanpää, M.: Preparation and characterization of a novel chitosan/Al2O3/magnetite nanoparticles composite adsorbent for kinetic, thermodynamic and isotherm studies of Methyl Orange adsorption. Chem. Eng. J. (2015). https://doi.org/10.1016/j.cej.2014.07.109
47. Sizirici, B., Yildiz, I.: Adsorption capacity of iron oxide-coated gravel for landfill leachate: simultaneous study. Int. J. Environ. Sci. Technol. (2017). https://doi.org/10.1007/s13762-016-1207-9
48. Aly, Z., Graulet, A., Scales, N., Hanley, T.: Removal of aluminium from aqueous solutions using PAN-based adsorbents: characterisation, kinetics, equilibrium and thermodynamic studies. Environ. Sci. Pollut. Res. (2014). https://doi.org/10.1007/s11356-013-2305-6
49. Lagergen, S.K.: About the Theory of So-called Adsorption of Soluble Substances. Sven. Vetenskapsakad, Handingarl (1898)
50. Negm, N.A., Abd El Wahed, M.G., Hassan, A.R.A., Abou Kana, M.T.H., Feasibility of metal adsorption using brown algae and fungi: Effect of biosorbents structure on adsorption isotherm and kinetics, J. Mol. Liq. (2018). https://doi.org/10.1016/j.molliq.2018.05.027
51. Idris, S.A., Alotaibi, K.M., Peshkur, T.A., Anderson, P., Morris, M., Gibson, L.T.: Adsorption kinetic study: Effect of adsorbent pore size distribution on the rate of Cr(VI) uptake. Micropor. Mesopor. Mat. (2013). https://doi.org/10.1016/j.micromeso.2012.08.001
52. Repo, E., Warchoł, J.K., Bhatnagar, A., Mudhoo, A., Sillanpää, M.: Aminopolycarboxylic acid functionalized adsorbents for heavy metals removal from water. Water Res. (2013). https://doi.org/10.1016/j.watres.2013.06.020
53. Chaudry, S.A., Khan, T.A., Ali, I.: Adsorptive removal of Pb(II) and Zn(II) from water onto manganese oxide-coated sand: Isotherm, thermodynamic and kinetic studies. Egypt. J. Basic Appl. Sci. (2016). https://doi.org/10.1016/j.ejbas.2016.06.002
54. Changmai, M., Priyesh, J.P., Purkait, M.K.: Al_2O_3 nanoparticles synthesized using various oxidizing agents: Defluoridation performance. Journal of Science: Advanced Materials and Devices (2017). https://doi.org/10.1016/j.jsamd.2017.09.001
55. Shekarriz, M., Ramezani, Z., Elhami, F.: Preparation and characterization of ZSM5-supported nano-zero-valent iron and its potential application in nitrate remediation from aqueous solution. Int. J. Environ. Sci. Technol. (2017). https://doi.org/10.1007/s13762-016-1213-y
56. Hameed, B.H.: Removal of cationic dye from aqueous solution using jackfruit peel as non-conventional low-cost adsorbent. J. Hazard. Mater. (2009). https://doi.org/10.1016/j.jhazmat.2008.05.045
57. Cheung, W.H., Szeto, Y.S., McKay, G.: Intraparticle diffusion processes during acid dye adsorption onto chitosan. Bioresour. Technol. (2007). https://doi.org/10.1016/j.biortech.2006.09.045
58. Ofomaja, A.E.: Kinetics and mechanism of methylene blue sorption onto palm kernel fibre. Process Biochem. (2007). https://doi.org/10.1016/j.procbio.2006.07.005